Journal of Crystal Growth 310 (2008) 3224–3229

Contents lists available at ScienceDirect

Journal of Crystal Growth

journal homepage: www.elsevier.com/locate/jcrysgro

Characterization and properties of infrared NLO crystals: $AGeX_3$ (A = Rb, Cs; X = Cl, Br)

Zhi-Guang Lin [a,*], Li-Chuan Tang [b], Chang-Pin Chou [a]

[a] Department of Mechanical Engineering, National Chiao Tung University, Hsinchu 305, Taiwan, ROC
[b] Department of Electrical Engineering, Chung-Cheng Institute of Technology, National Defense University, Taoyuan 353, Taiwan, ROC

ARTICLE INFO

Available online 13 March 2008

PACS:
61.50.Nw
61.66.Fn

Keywords:
A1. Optical characterization
A1. Solid solutions
A2. Growth from solutions
B1. Halides
B2. Nonlinear optic materials

ABSTRACT

Innovative infrared nonlinear optical crystals $AGeX_3$ were synthesized. Their powder X-ray diffraction patterns demonstrated that they had rhombohedral structures with R3m (no. 160) space group symmetry (except $RbGeBr_3$). Their structural distortion increased with Br content, but decreased with Rb content. The Kurtz powder methods revealed that the nonlinear optical efficiency of $CsGeBr_3$ is 9.64 times that of rhombohedral $CsGeCl_3$ and 28.29 times that of KDP; most importantly, $AGeX_3$ is phase-matchable (except $RbGeBr_3$).

1. Introduction

Second-order nonlinear optical (NLO) materials played a key role in such optical fields as laser frequency conversion and optical parametric oscillation/amplification (OPO/OPA) [1,2]. For inorganic second-order NLO materials, several crystals used in ultraviolet (UV) and visible regions were proposed in the past two decades, such as KH_2PO_4 (KDP), $KTiOPO_4$ (KTP), β-BaB_2O_4 (BBO), LiB_3O_5 (LBO). But in the infrared (IR) region the current materials, such as $AgGaSe_2$, $ZnGeP_2$, are not good enough for applications mainly due to their low laser damage threshold, as their band gaps were smaller than 1.5 eV. Therefore, the search for new NLO crystals with excellent properties, especially a high damage threshold, has become a key area of research in NLO material science and laser technology [3].

Cesium trihalometalates $CsMX_3$ of group-IV elements (M = Ge, Sn, Pb; X = Cl, Br, I) have M^{2+} (ns^2) cations and crystallize in perovskite variants [4–10]. Under ambient conditions $CsMX_3$ adopts a rhombohedral structure, an attractive nonlinear crystal, which is applied in the infrared region. Since the optical damage threshold and the range of transparency of materials are related to the magnitude of the band gap, and the optical nonlinearity is inversely proportional to the cube of the band gap [11]. The linear and NLO properties of $CsGe(Br_xCl_{1-x})_3$ and $(Rb_yCs_{1-y})GeBr_3$ can be adjusted by varying the alloy composition to satisfy the demand for specific applications. This investigation presents a method for synthesizing crystals and measuring the optical properties for each composition. Nonlinear coefficients of $CsGe(Br_xCl_{1-x})_3$, $x = 0, \frac{1}{4}, \frac{2}{4}, \frac{3}{4}, 1$ and $y = 0, \frac{1}{4}, \frac{2}{4}, \frac{3}{4}, 1$ are also considered to reveal the potential of these crystals in NLO applications.

2. Experimental details

2.1. Synthesis

The synthetic procedure was modified from that of Gu et al. [12–14]. Chritensen and Rasmussen [15] and Tananaev et al. [16] used different synthetic methods, but their methods seemed complex and offered poor productivity. In this work, H_3PO_2 (50%) was loaded with HBr (48%), HCl (37%) and GeO_2 (99.999%) into a 250 ml beaker, and then heated to 95 °C. The solution was vigorously mixed for 5 hours and then cooled to room temperature. After the precipitate was removed, CsBr (99.9%) and RbBr (99.8%) were added and the temperature was raised to the boiling point; the mixture was then naturally cooled to room temperature. A light yellow precipitate was formed. The reaction equations were as follows:

$$H_3PO_2 + 6xHBr + 6(1-x)HCl + 2GeO_2 = H_3PO_4 + 2HGe(Br_xCl_{1-x})_3 + 2H_2O$$

* Corresponding author. Tel.: +886 3 5712121 55157; fax: +886 3 5720634.
E-mail address: zglin.me91g@nctu.edu.tw (Z.-G. Lin).

0022-0248/$ - see front matter © 2008 Elsevier B.V. All rights reserved.
doi:10.1016/j.jcrysgro.2008.03.018

then

$$HGe(Br_xCl_{1-x})_3 + CsBr = CsGe(Br_xCl_{1-x})_3\downarrow + HBr$$

and

$$H_3PO_2 + 6HBr + 2GeO_2 = H_3PO_4 + 2HGeBr_3 + 2H_2O$$

then

$$HGeBr_3 + yRbBr + (1-y)CsBr = (Rb_yCs_{1-y})GeBr_3\downarrow + HBr$$

Recrystallization was performed by mixing the precipitate with 1:1 concentrated HX and alcohol solution to yield yellow crystals of $CsGe(Br_xCl_{1-x})_3$ and $(Rb_yCs_{1-y})GeBr_3$. This approach was performed 7 times to ensure no residual precursor remained. Then, the crystals were dried at 85 °C for 48 hours under a vacuum to prevent any effect of the deliquescence on them. The color of the precipitated product varied from yellow to white as soon as the substituted ratio, x, changed from 1 to 0.

2.2. Physical measurements

Rhombohedral crystals were synthesized and sieved into particles of different sizes to measure and analyze its structural and optical properties. The crystalline structures were observed using an X-ray diffractometer. The composition of all of the samples was measured by electron-probe X-ray microanalysis (EPMA). Raman spectra were obtained to determine the atomic vibration. The absorption edge was measured using a UV-visible spectrometer. Linear optical properties were measured using an ellipsometer. NLO properties were determined by making powder second-harmonic generation measurements.

3. Results and discussion

3.1. Composition and structural properties

Fig. 1 presents the composition of $CsGe(Br_xCl_{1-x})_3$, ($x = 0, \frac{1}{4}, \frac{2}{4}, \frac{3}{4}, 1$) and $(Rb_yCs_{1-y})GeBr_3$ ($y = 0, \frac{1}{4}, \frac{2}{4}, \frac{3}{4}, 1$) obtained from EPMA measurements. These results indicate that those samples had a Cs to Ge ratio of almost 1:1 (for CGBC) and Ge to Br ratio of almost 1:3 (for RCGB). EPMA measurement qualitatively verified that chlorine atoms were successfully doped in the $CsGeBr_3$ crystal and rubidium atoms were also successfully doped in the $CsGeBr_3$ crystal. Although it still contained some impurities, they are all smaller than 1% ($O_{max} \leqslant 0.52\%$, $P_{max} \leqslant 0.61\%$).

X-ray diffraction was employed to determine the structural parameters of all the crystals $CsGe(Br_xCl_{1-x})_3$ and $(Rb_yCs_{1-y})GeBr_3$. The synthesized crystals were crushed, ground and sieved. X-ray diffractograms were obtained at room temperature using Cu-Kα radiation with Siemens D5000 equipment. From Fig. 2, the substitution-related diffraction peaks shifted gradually with substituted content for the anion substituted crystals. An extra CsBr crystal was used as an internal standard to determine the lattice parameters. The measured pattern was indexed and analyzed, as in the full-profile Rietveld refinement, using the nonprofit program *PowderCell* [17], which was developed by Kraus and Nolze. The structural parameters of $CsGe(Br_xCl_{1-x})_3$ and $(Rb_yCs_{1-y})GeBr_3$ were compared with those of $CsGeCl_3$ (R3m, no.160), $CsGeBr_3$ (R3m, no.160) and $RbGeBr_3$ (Pn21a, no.33), which

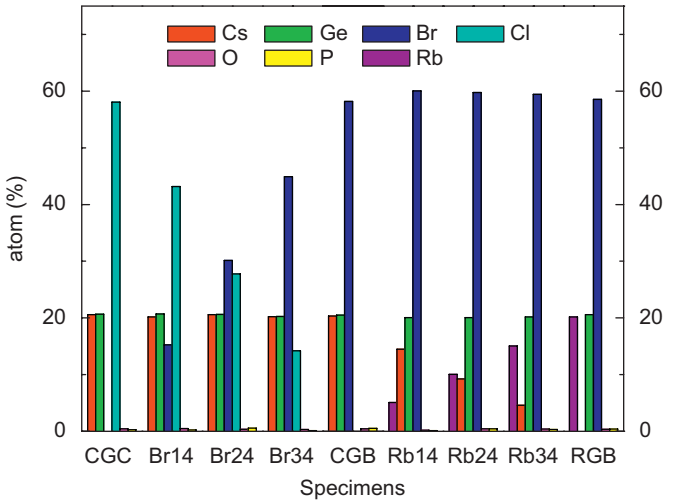

Fig. 1. EPMA measurements, $CsGe(Br_xCl_{1-x})_3$: $x = 0, \frac{1}{4}, \frac{2}{4}, \frac{3}{4}, 1$ and $(Rb_yCs_{1-y})GeBr_3$:$y = 0, \frac{1}{4}, \frac{2}{4}, \frac{3}{4}, 1$.

were presented in JCPDS. The peak-splitting caused by structural non-centrosymmetry, occurs mainly from $2\theta = 15^\circ$ to 35° (Fig. 2). The X-ray diffraction peaks shifted gradually as the substituted composition changed. Certain strong diffraction peaks were observed at $2\theta = 31.76^\circ$, 27.66°, 26.86°, 22.60°, 22.10°, 15.76° in $CsGeBr_3$. These diffraction patterns were compared with those with JCPDS and were indexed (2 0 0), (1 $\bar{1}$ 1), (1 1 1), (1 $\bar{1}$ 0), (1 1 0) and (1 0 0) planes, respectively. The XRD patterns also verify that $CsGe(Br_xCl_{1-x})_3$ ($x = 0, \frac{1}{4}, \frac{2}{4}, \frac{3}{4}, 1$) and $(Rb_yCs_{1-y})GeBr_3$ ($y = 0, \frac{1}{4}, \frac{2}{4}, \frac{3}{4}$) crystallized in the non-centrosymmetric [18] rhombohedral space group R3m.

In an ideal perovskite structure, the cell parameters were $a = b = c$ and $\alpha = \beta = \gamma = 90^\circ$ with cubic space group $Pm\bar{3}m$ (no. 221). Examples are the high-temperature phase of cubic $CsGeCl_3$ and $CsGeBr_3$ [18–22]: the cell parameters of cubic $CsGeBr_3$ are $a = b = c = 5.362$ Å and $\alpha = \beta = \gamma = 90^\circ$. The cell edges of rhombohedral (room temperature phase) $CsGeBr_3$ were longer than those of cubic (high-temperature) phase, and the cell angles of rhombohedral (room temperature phase) $CsGeBr_3$ were slightly smaller than 90°. The structural distortion contributes to the optical nonlinearity of $CsGeBr_3$. Structural parameters from Fig. 3 indicated that the lattice constant increased with Br content and the cell angle became smaller. Therefore, the structural distortion of $CsGe(Br_xCl_{1-x})_3$ (R3m) increases with Br content. In contrast, the lattice constant became smaller as the Rb content increased while the cell angle became larger. Hence, the structure of $(Rb_yCs_{1-y})GeBr_3$ gradually becomes centrosymmetric as Rb content increases.

3.2. Linear optical properties

Fig. 4 shows the absorption spectra obtained at room temperature using $CsGe(Br_xCl_{1x})_3$ ($x = 0, \frac{1}{4}, \frac{2}{4}, \frac{3}{4}, 1$) and $(Rb_yCs_{1-y})GeBr_3$ ($y = 0, \frac{1}{4}, \frac{2}{4}, \frac{3}{4}, 1$) crystals in the UV-visible light range. Thin plates ($\approx 500\,\mu m$) of $CsGe(Br_xCl_{1-x})_3$ and $(Rb_yCs_{1-y})GeBr_3$ were used to make the band gap measurements. The recorded curves can be approximated as straight lines for α^2 against $h\nu$, where α is the absorption coefficient and $h\nu$ is the photon energy. The straight-line approximation is applied to the rapidly increasing portions of the curves in Fig. 4. Hence, the fundamental absorption edge is described by $\alpha = A(h\nu - E_g)^{1/2}$, where A is a constant and the band gap E_g can be determined the points of intersection of the straight lines with the abscissa. This dependence corresponds to directly

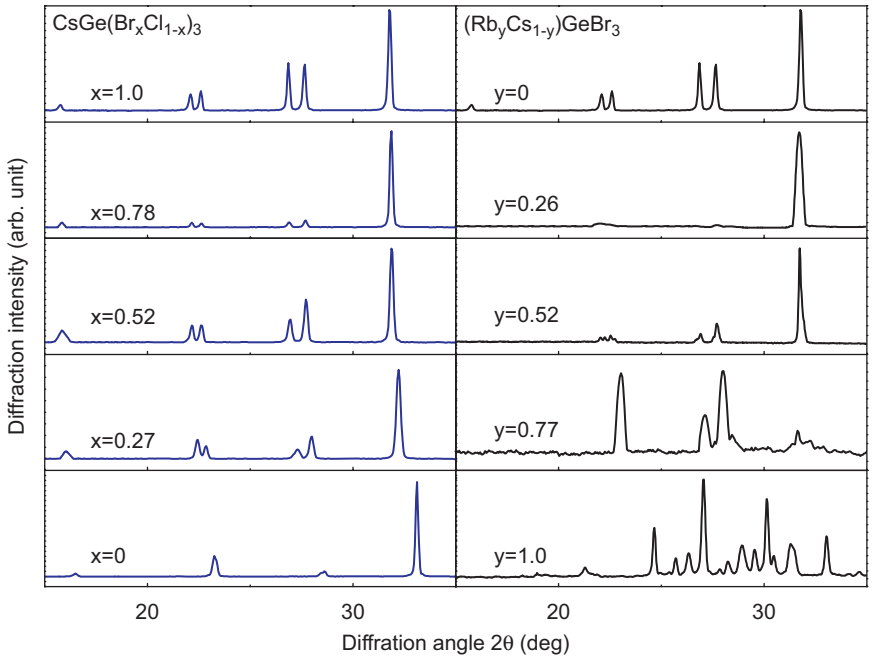

Fig. 2. X-ray powder diffraction for the NLO crystals $CsGe(Br_xCl_{1-x})_3$ and $(Rb_yCs_{1-y})GeBr_3$.

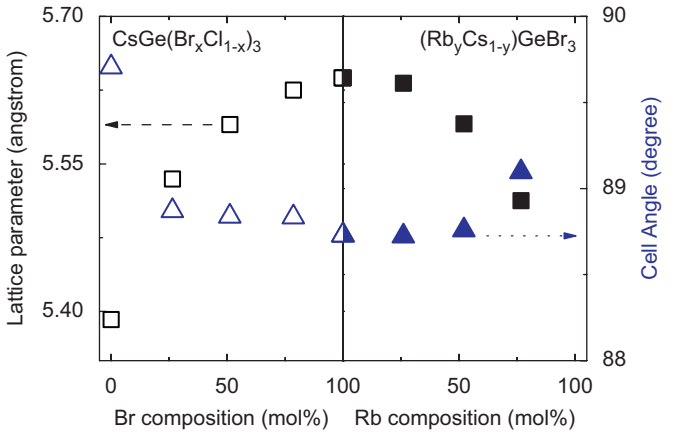

Fig. 3. Structural parameters of the NLO crystals $CsGe(Br_xCl_{1-x})_3$ and $(Rb_yCs_{1-y})GeBr_3$.

allowed electronic transitions [23]. In the inset in Fig. 4, the band gap values are plotted versus substituted content. Although the absorption edge declines from 3.43 to 2.38 eV as the bromine content ($x = 0$–1), the absorption edge remains fixed for $y = 0$–$\frac{3}{4}$.

In the Raman scattering measurement, the $CsGe(Br_xCl_{1-x})_3$ and $(Rb_yCs_{1-y})GeBr_3$ samples were illuminated at room temperature using an argon ion laser at 488 nm at an average power of 30 mW. Fig. 5 plots the results. The Raman peaks shift as the Br content, which fact is consistent with the fact that the phonon frequency is inversely proportional to the square root of the mass of GeX_3 (X = Cl, Br). Our data agree closely with the Raman spectra of $CsGeCl_3$ and $CsGeBr_3$ proposed by Thiele et al. [21]. The strongest Raman peaks are associated with the A_1 mode. Raman peaks at 264–292 cm^{-1} can be also attributed to the A_1 mode. Another group of Raman peaks (from 159 to 164 cm^{-1}) is associated with the E mode. The other group of Raman peaks (from 207 to 237 cm^{-1}) can be attributed to the A_1+E mode and the A_1 mode for $CsGe(Br_xCl_{1-x})_3$ and $(Rb_yCs_{1-y})GeBr_3$, respectively. Raman peaks of $CsGeBr_3$ at 419.21 and 209.79 cm^{-1} are associated with the corresponding (50.5 cm^{-1}) overtones. Raman peaks of $CsGeCl_3$ at 236.98 cm^{-1} can be assigned to the corresponding (58.5 cm^{-1}) overtone. From Fig. 6, lines (2–5,7) are associated with the anion substitution. Line (5) is associated with bromine atoms while line (7) relates to only chlorine atoms. Lines (2–4) are related to Ge–X_3 bonds. This result is consistent with the effective-mass concept: the oscillation frequency is expected to increase as the Br content declines because the Br atom is heavier than Cl. Lines (1,6,8) are attributed to the oscillation between Cs^+ and $Ge(Br_xCl_{1-x})_3^{-1}$ because they are less influenced by the anion substitution. In line (6), Raman signals were changed from the anion vibration A_1+E modes to the cation vibration A_1 modes, revealing that the relative vibration between Cs^+ and the anion cluster $Ge(Br_xCl_{1-x})_3^{-1}$ was transformed to the doubly degenerate vibration of Ge–Br bonds.

3.3. Nonlinear optical properties

Powder SHG measurements, which were made by Chen et al. [24], were made herein using a modified Kurtz-NLO system [25] with 1260 nm light. A mode-locked Cr^{4+}: Forsterite femtosecond laser with a pulse duration of 50 fs, was used in all measurements. The Cr^{4+}: Forsterite oscillator yields pulses with a typical FWHM bandwidth of about 45 nm at a repetition rate of 76 MHz and an average power of 270 mW. Since the SHG efficiency of powders has been shown to depend strongly on particle size [25,26], crystals were ground and sieved (Newark Wire Cloth Company) into six particle-size ranges −19–37, 37–74, 74–105, 105–210, 210–420 and 420–840 μm. Crystalline KDP was also ground and sieved into the same particle-size ranges to support relevant comparison with known SHG materials. All of the powders were placed in separate capillary tubes. The

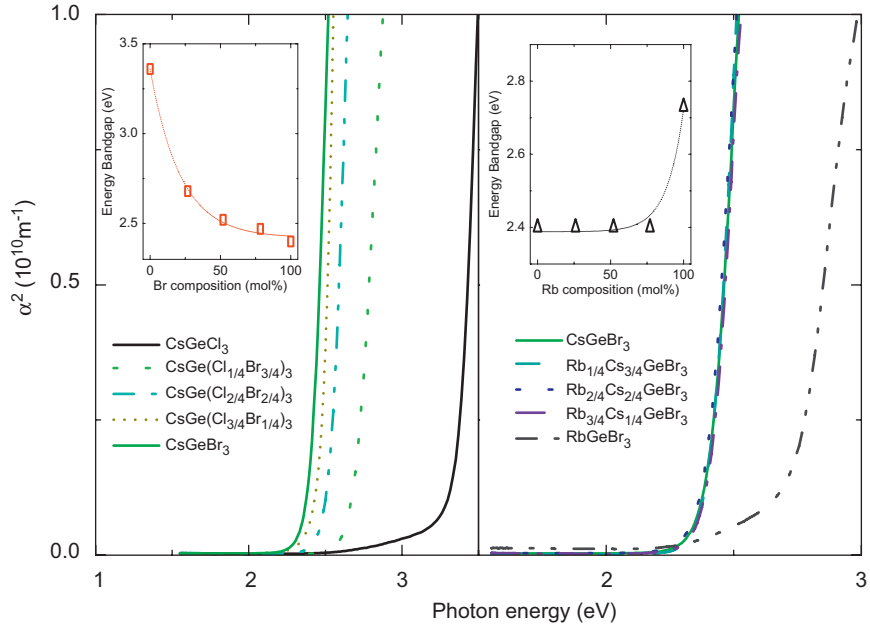

Fig. 4. Absorption coefficient near the band edge of $CsGe(Br_xCl_{1-x})_3$ and $(Rb_yCs_{1-y})GeBr_3$ plotted in coordinates α^2 and $h\nu$. The inset shows the substituted composition dependence of E_g obtained.

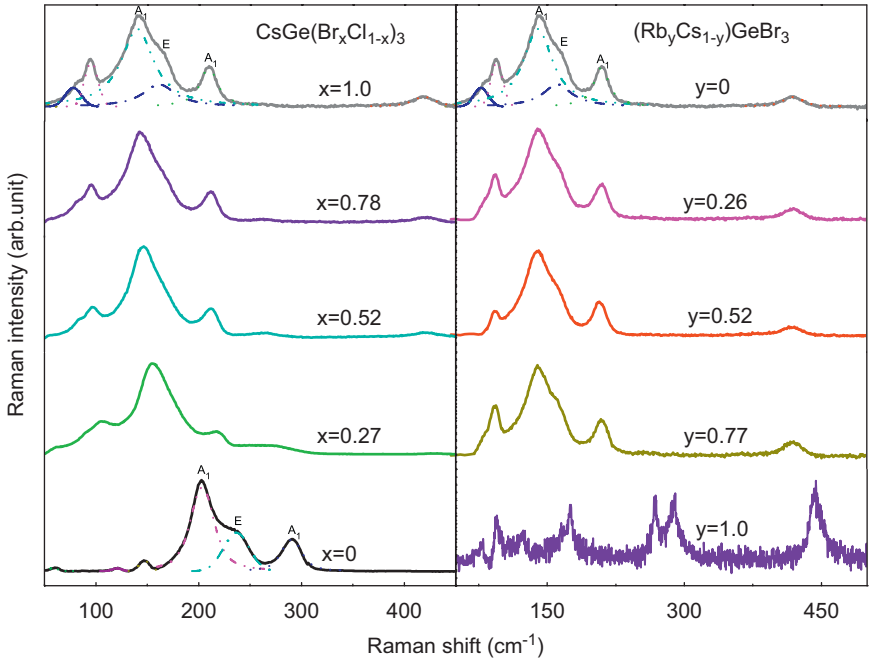

Fig. 5. Raman spectrum of $CsGe(Br_xCl_{1-x})_3$ and $(Rb_yCs_{1-y})GeBr_3$ crystals at room temperature.

SHG radiation (630 nm) was collected in transmission and detected using a photomultiplier tube (Oriel Instruments). The SHG signal was collected by a data-acquisition (DAQ) interface and was monitored using an analysis program on a personal computer.

Powder SHG measurements of sieved polycrystalline $CsGe(Br_xCl_{1-x})_3$ and $(Rb_yCs_{1-y})GeBr_3$ (Fig. 7) demonstrated that the SHG efficiencies of all the samples exceeded that of KDP. Moreover, all of them were phase-matchable, as was KDP, such that as the particles became substantially larger than the coherence length of the crystal, and the collected SHG intensity no longer increased, saturating at a particular value. The saturated PSHG intensities were estimated from the transmission signals in particle of various sizes, indicating that the SHG responses were strengthened as the Br content increased, but decayed as the Rb content increased. The d_{eff} values were calculated (by $d_{KDP} = 0.36$ pm/V [10]) and are plotted in Fig. 8. The effective

powder second-harmonic generation coefficients increased with Br content, but decreased as the Rb content increased. Some reasons exist for the significant SHG signals of rhombohedral $CsGe(Br_xCl_{1-x})_3$ and $(Rb_yCs_{1-y})GeBr_3$ crystals. First, the structural distortion and the off-center Ge ion in the unit cell contributed to the SHG responses. The XRD results indicated that the structural distortion increased with Br content but decreased with Rb content. And the cell angle became smaller as Br content increased but became larger as Rb content increased. The position of the B-site cation, Ge, moved closer to the cell corner as the Br increased. Then, the nonlinearity increased with Br content, but declined as Rb content increased. Second, the optical nonlinearity is approximately inversely proportional to the cube of the band gap value [11]. Therefore, the band gap values fell and the NLO susceptibilities increased with the atomic weights of the halides.

4. Conclusions

The structural and optical properties of rhombohedral NLO crystals, $CsGe(Br_xCl_{1-x})_3$ ($x = 0, \frac{1}{4}, \frac{2}{4}, \frac{3}{4}$ and 1) and $(Rb_yCs_{1-y})GeBr_3$ ($x = 0, \frac{1}{4}, \frac{2}{4}$ and $\frac{3}{4}$), have been investigated experimentally to reveal the substitution effect. Based on the results, the linearly increasing x increases lattice constant and second-order NLO susceptibility; but reduces the cell angle and the band gap values. The linearly increasing y yields opposite results. Owing to the optical damage threshold and the range of transparency of materials are related to the magnitude of the band gap, and the optical nonlinearity is inversely proportional to the cube of the band gap [11], the properties of halides could be modulated by anion substitution, but not cation substitution.

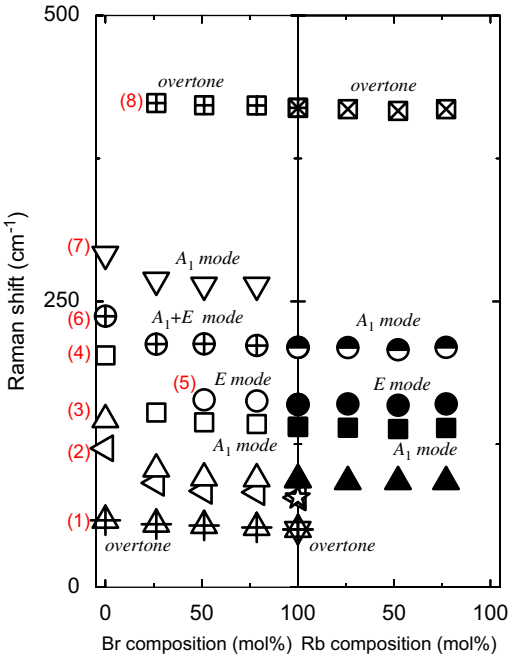

Fig. 6. Raman vibrational modes of $CsGe(Br_xCl_{1-x})_3$ (R3m) and $(Rb_yCs_{1-y})GeBr_3$ (R3m) crystals.

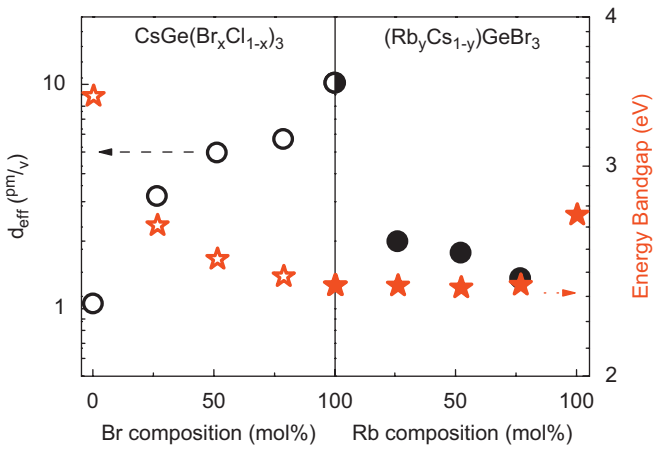

Fig. 8. The effective powder second-harmonic generation coefficients of nonlinear optical crystals $CsGe(Br_xCl_{1-x})_3$ and $(Rb_yCs_{1-y})GeBr_3$ and their energy band gaps.

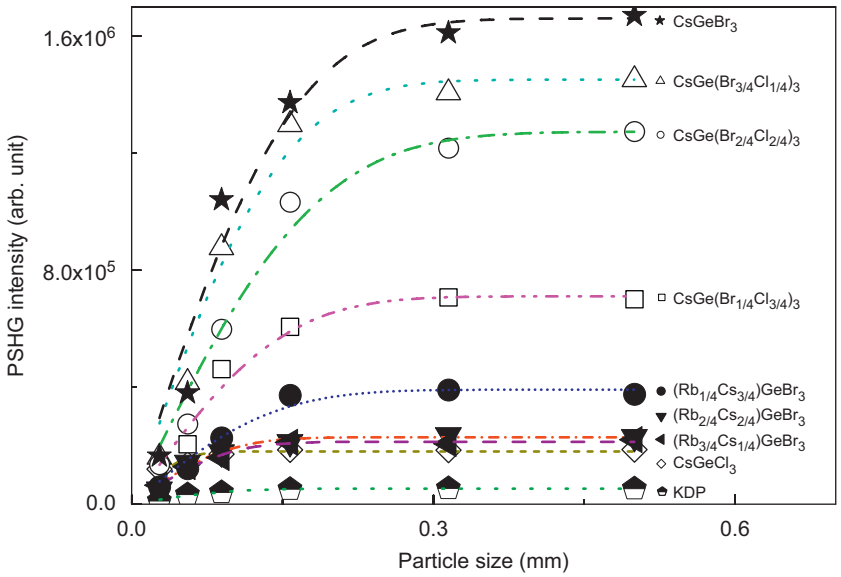

Fig. 7. The comparison of integrated powder second-harmonic generation intensity of nonlinear optical crystals KDP, $CsGe(Br_xCl_{1-x})_3$ and $(Rb_yCs_{1-y})GeBr_3$.

Acknowledgments

The authors would like to thank the National Science Council of the Republic of China, Taiwan, for financially supporting this research under Contract no. NSC 95-2112-M-009-042.

References

[1] D.M. Burland, Chem. Rev. 94 (1994) 1.
[2] D.S. Chemla, J. Zyss, Nonlinear Optical Properties of Organic Molecules and Crystals, Academic Press, Orlando, 1987.
[3] V.G. Dmitriev, G.G. Gurzadyan, D.N. Nikogosyan, Handbook of Nonlinear Optical Crystals, third ed, Springer, Berlin, 1999.
[4] J. Zhang, PhD thesis, Department of Material Science, Wuhan University, 1995.
[5] M.D. Ewbank, F. Cunningham, R. Borwick, M.J. Rosker, P. Gunter, CLEO'97: Summaries of Papers Presented at the Conference on Lasers and Electro-Optics, vol. 11, 1997, 462pp.
[6] J. Zhang, N. Su, C. Yang, J. Qin, N. Ye, B. Wu, C. Chen, Chem. Proc. SPIE 3556 (1998) 1.
[7] L.C. Tang, C.S. Chang, J.Y. Huang, J. Phys.: Condens. Matter 12 (2000) 9129.
[8] P. Ren, J. Qin, C. Chen, Inorg. Chem. 42 (2003) 8.
[9] P. Ren, J. Qin, T. Liu, Y. Wu, C. Chen, Optic. Mater. 23 (2003) 331.
[10] L.C. Tang, J.Y. Huang, C.S. Chang, M.H. Lee, L.Q. Liu, J. Phys.: Condens. Matter 17 (2005) 7275.
[11] Y.R. Shen, The Principles of Nonlinear Optics, Wiley, New York, 2002.
[12] Q. Gu, Q. Pan, W. Shi, X. Sun, C. Fang, Prog. Cryst. Growth Charact. Mater. 40 (2000) 89.
[13] Q. Gu, Q. Pan, X. Wu, W. Shi, C. Fang, J. Crystal Growth 212 (2000) 605.
[14] Q. Gu, C. Fang, W. Shi, X. Wu, Q. Pan, J. Crystal Growth 225 (2001) 501.
[15] A.N. Christensen, S.E. Rasmussen, Acta Chem. Scand. 19 (1965) 421.
[16] I.V. Tananaev, D.F. Dzhurinskii, Y.N. Mikhailov, Zh. Neorgan. Khim. 9 (1964) 1570.
[17] W. Kraus, G. Nolze, J. Appl. Crystallogr. 29 (1996) 301.
[18] D.K. Seo, N. Gupta, M.H. Whangbo, H. Hillebrecht, G. Thiele, Inorg. Chem. 37 (1998) 407.
[19] U. Schwarz, H. Hillebrecht, M. Kaupp, K. Syassen, H.G. von Schnering, G. Thiele, J. Solid State Chem. 118 (1995) 20.
[20] U. Schwarz, F. Wagner, K. Syassen, H. Hillebrecht, Phys. Rev. B 53 (1996) 12545.
[21] G. Thiele, H.W. Rotter, K.D. Schmidt, Z. Anorg, Allg. Chem. 545 (1987) 148.
[22] G. Thiele, H.W. Rotter, K.D. Schmidt, Z. Anorg, Allg. Chem. 559 (1988) 7.
[23] J.I. Pankove, Optical Processes in Semiconductors, Prentice-Hall, Englewood Cliffs, NJ, 1971.
[24] W.K. Chen, C.M. Cheng, J.Y. Huang, W.F. Hsieh, T.Y. Tseng, J. Phys. Chem. Solids 61 (2000) 969.
[25] S.K. Kurtz, T.T. Perry, J. Appl. Phys. 39 (1968) 3798.
[26] J.P. Dougherty, S.K. Kurtz, J. Appl. Crystallogr. 9 (1976) 145.